Drosophila Kelch regulates actin organization via Src64-dependent tyrosine phosphorylation

Reed J. Kelso,[1] Andrew M. Hudson,[2] and Lynn Cooley[1,2]

[1]Department of Cell Biology and [2]Department of Genetics, Yale University School of Medicine, New Haven, CT 06520

The *Drosophila kelch* gene encodes a member of a protein superfamily defined by the presence of kelch repeats. In *Drosophila*, Kelch is required to maintain actin organization in ovarian ring canals. We set out to study the actin cross-linking activity of Kelch and how Kelch function is regulated. Biochemical studies using purified, recombinant Kelch protein showed that full-length Kelch bundles actin filaments, and kelch repeat 5 contains the actin binding site. Two-dimensional electrophoresis demonstrated that Kelch is tyrosine phosphorylated in a *src64*-dependent pathway. Site-directed mutagenesis determined that tyrosine residue 627 is phosphorylated. A Kelch mutant with tyrosine 627 changed to alanine (KelY627A) rescued the actin disorganization phenotype of *kelch* mutant ring canals, but failed to produce wild-type ring canals. Electron microscopy demonstrated that phosphorylation of Kelch is critical for the proper morphogenesis of actin during ring canal growth, and presence of the non-phosphorylatable KelY627A protein phenocopied *src64* ring canals. KelY627A protein in ring canals also dramatically reduced the rate of actin monomer exchange. The phenotypes caused by *src64* mutants and KelY627A expression suggest that a major function of Src64 signaling in the ring canal is the negative regulation of actin cross-linking by Kelch.

Introduction

Although much is known about the key elements in actin filament formation and regulation in vitro (Pollard et al., 2000), our understanding of temporal and spatial regulation of actin dynamics in vivo is far from complete. Observations of actin dynamics at the leading edges of migrating cells have begun to describe the in vivo kinetics of actin assembly during cell migration (for review see Condeelis, 2001; Pantaloni et al., 2001). *Dictyostelium* and the budding yeast *Saccharomyces cerevisiae* have both proved to be valuable in the in vivo characterization of components involved in regulation of the actin cytoskeleton (for review see Noegel and Schleicher, 2000; Pruyne and Bretscher, 2000). We are able to combine microscopic studies of large actin structures with the expansive palate of genetic tools available in *Drosophila* to examine the regulation of F-actin in the ovarian ring canal.

In *Drosophila melanogaster*, 15 syncytial nurse cells and 1 oocyte are enveloped by a monolayer of somatic follicle cells and constitutes an egg chamber, the structural and functional unit of the *Drosophila* ovary (for review see Spradling, 1993). A ring canal is a gateway through which mRNAs, proteins, and nutrients flow from nurse cells into the oocyte during the entire course of oogenesis. Ring canals are derived from arrested mitotic cleavage furrows that are modified by the addition of several proteins. These include abundant F-actin (Koch and King, 1969), at least one protein that is recognized by antiphosphotyrosine antibodies (PY protein), a mucin-like glycoprotein (Kramerova and Kramerov, 1999), the Hts ring canal protein (HtsRC)* (Yue and Spradling, 1992; Robinson et al., 1994), ABP280/filamin (Li et al., 1999; Sokol and Cooley, 1999), Tec29 and Src64 tyrosine kinases (Dodson et al., 1998; Roulier et al., 1998), and Kelch (Xue and Cooley, 1993; Robinson and Cooley, 1997a).

As nurse cell cytoplasm transport proceeds, the diameter of ring canals grows from <1 μm to 10–12 μm. This represents the addition of over one inch of filamentous actin during a period in which the filament density remains constant (Tilney et al., 1996). Near the end of oogenesis, the ring canal actin transforms from a single continuous bundle into several interwoven actin cables (Tilney et al., 1996). Ring canal expansion probably involves the nucleation of

Address correspondence to Lynn Cooley, Department of Genetics, Yale University School of Medicine, P.O. Box 208005, New Haven, CT 06520-8005. Tel.: (203) 785-5067. Fax: (203) 785-6333. E-mail: lynn.cooley@yale.edu

Key words: oogenesis; kelch; Src; actin binding; ring canal

*Abbreviations used in this paper: 2D, two-dimensional; BTB, broad complex, tramtrack, and bric-á-brac; FRAP, fluorescence recovery after photobleaching; GFP, green fluorescent protein; HtsRC, Hts ring canal protein; KREP, kelch repeat; POZ, poxvirus and zinc finger; SFK, Src family kinase.

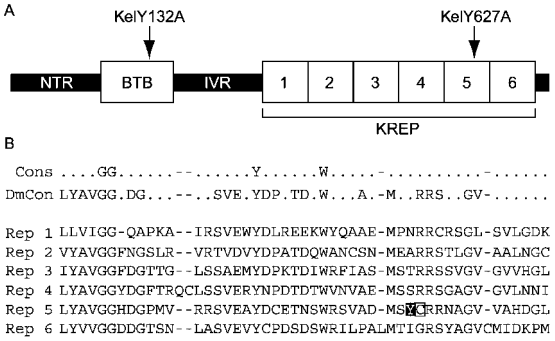

Figure 1. **Domain organization of *Drosophila* kelch.** (A) Kelch has four protein domains: amino-terminal region (NTR), BTB domain, intervening region (IVR), and KREP. The NTR regulates the timing of Kelch localization to the ring canal (Robinson and Cooley, 1997a). The BTB (or POZ) domain mediates dimerization of full-length Kelch. The KREP domain, composed of six tandem repeats, is required for localization of Kelch to ring canals. Two candidate phosphotyrosine residues are predicted to occur in Kelch: one in the BTB at position 132 and the other in KREP at position 627. Site-directed mutations of these residues are designated KelY132A and KelY627A. (B) A closer look at the sequences of each of the six KREPs shows that residue 627 (shaded) occurs within the same repeat (Rep 5) that has been described as the actin-binding repeat of *Limulus* α-scruin based on the chemical reactivity of the neighboring cysteine (boxed residue; Sun et al., 1997). The alignment also shows that the tyrosine residue present in the fifth repeat is not present in the five other *Drosophila* repeats.

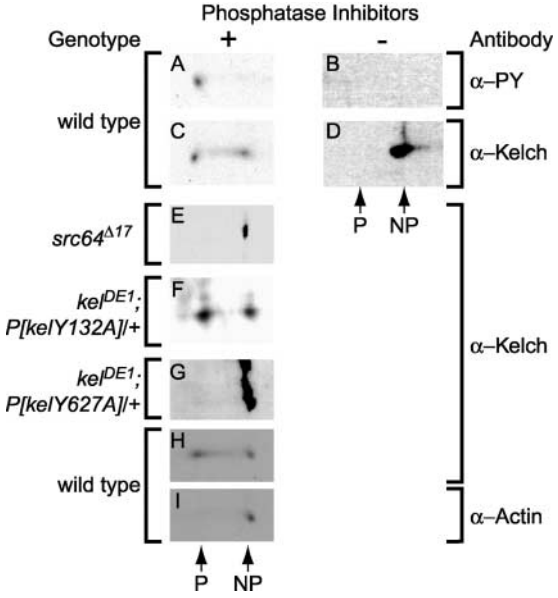

Figure 2. **2D electrophoresis performed in the presence (+) or absence (−) of phosphatase inhibitors.** (A) Wild-type egg chambers have a phosphotyrosine reactive spot in the presence of phosphatase inhibitors that comigrates with one of the two Kelch spots (C). (B and D) In the absence of phosphatase inhibitors, only the nonphosphorylated Kelch isoform is detected. (E) In *src64*$^{\Delta 17}$ homozygous egg chambers, only the nonphosphorylated Kelch isoform is detected. (F) *kel*^{DE1};*P[kelY132A]*/+ egg chambers have both isoforms of Kelch. (G) *kel*^{DE1};*P[kelY627A]*/+ egg chambers have only the nonphosphorylated isoform of Kelch. Blots of wild-type extracts incubated with actin and then probed with anti-kelch antibody (H) or anti-actin antibody (I) showed that actin was bound only to the nonphosphorylated form of Kelch. NP, nonphosphorylated Kelch; P, phosphorylated Kelch.

new actin filaments and an increase in actin filament length, coupled with filament reorganization that requires the establishment of reversible actin cross-links.

Previous work has shown that the Kelch protein is required for ring canal morphogenesis (Xue and Cooley, 1993; Tilney et al., 1996; Robinson and Cooley, 1997a). Ring canal actin in *kelch* mutant egg chambers is severely disorganized and partially occludes the lumen. This leads to a defect in cytoplasm transport and the production of small, sterile eggs (Xue and Cooley, 1993). Kelch is a multidomain protein (Fig. 1 A) and a member of a superfamily of proteins defined, in part, by the presence of six 50–amino acid kelch repeats (KREPs). Based on sequence similarity to galactose oxidase, the KREP domain is predicted to fold into a six-bladed β-propeller (Bork and Doolittle, 1994; Adams et al., 2000). In *Limulus* the KREP domain is present in at least three scruin proteins, each of which contains two KREP domains (Way et al., 1995). The KREP domains of α-scruin each form an F-actin binding domain that allows α-scruin to act as an actin filament–cross-linking protein (Tilney, 1975; Bullitt et al., 1988; Sanders et al., 1996; Sun et al., 1997). Another KREP protein, Mayven, is found in human brain extracts and tightly colocalizes with F-actin in cultured human U373-MG astrocytoma/glioblastoma cells (Soltysik-Espanola et al., 1999). The second conserved domain in Kelch is the BTB/POZ (broad complex, tramtrack, and bric-á-brac; also known as the poxvirus and zinc finger domain) dimerization domain (Ahmad et al., 1998). The molecular makeup of the Kelch protein and the morphology of the *kelch* mutant ring canals suggest that Kelch could organize actin filaments by acting as a dimeric cross-linking protein (Robinson and Cooley, 1997a).

A signaling cascade that leads to malformed ring canals involves the Src family kinases (SFKs) Src64 and Tec29. SFKs are associated with the phosphorylation of several important proteins involved in regulating F-actin–rich structures including cell–substrate adhesions, cell–cell adhesions, and actin regulatory proteins such as p190 RhoGAP, cortactin, and ABP280/filamin (Brown and Cooper, 1996). *Src* mutations in mice result in osteoclasts deficient in the formation of ruffled borders and defective in forming the peripheral actin ring (Boyce et al., 1992; Schwartzberg et al., 1997). Mutations in *Drosophila src64* or *tec29* lead to small ring canals that lack most phosphotyrosine staining, and egg chambers that have incomplete nurse cell cytoplasm transport (Dodson et al., 1998; Guarnieri et al., 1998; Roulier et al., 1998).

Using a series of two-dimensional (2D) gel electrophoresis experiments, we determined that Kelch is phosphorylated in an SFK-dependent manner. We used site-directed mutagenesis to map the phosphorylated tyrosine residue. Thin section electron microscopy revealed striking differences in actin organization and filament number in lines expressing wild-type Kelch when compared with *src64*$^{\Delta 17}$ and the nonphosphorylatable form of Kelch. This showed that phosphorylation of Kelch is necessary for normal filament organization. Binding studies showed that the phosphorylated form of Kelch does not interact with actin. Therefore, Src64-mediated phosphorylation probably dissociates Kelch

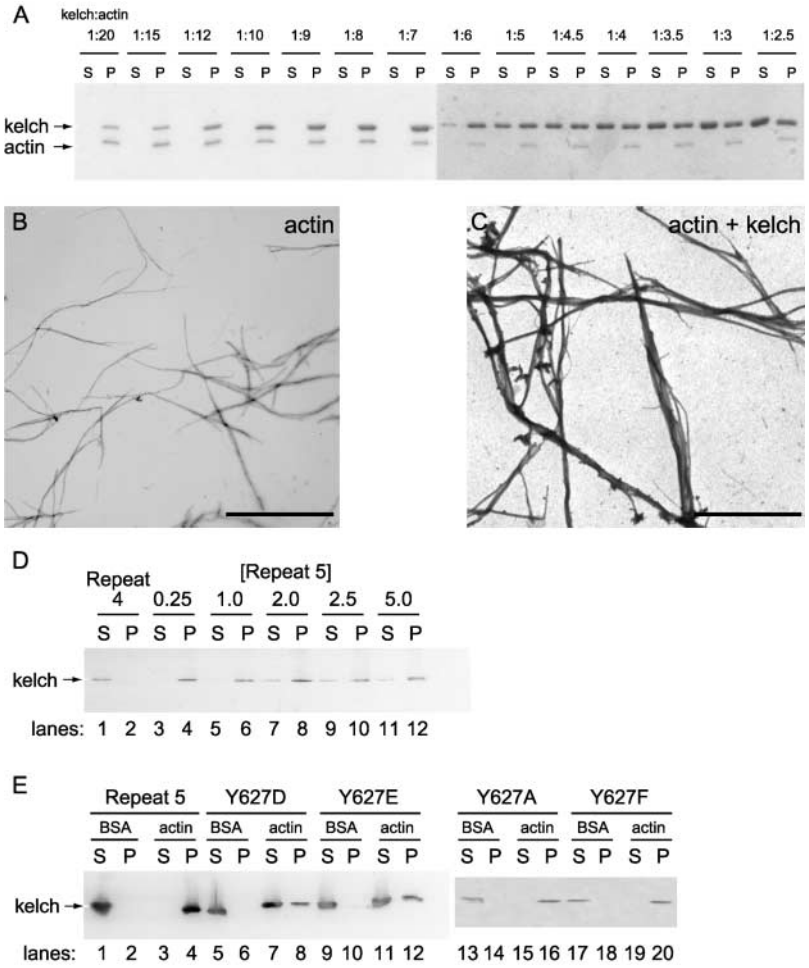

Figure 3. **F-actin binding assays with purified Kelch.** (A) Coomassie blue staining of SDS-PAGE gels containing the supernatants (S) and pellets (P) obtained when Kelch and F-actin were mixed in molar ratios varying from 1:20 to 1:2.5 (Kelch/actin) and centrifuged at 100,000 *g*. The concentration of phalloidin-stabilized F-actin was kept constant at 3 μM, and the concentrations of Kelch varied. (B) Electron micrographs of negatively stained F-actin. (C) Negatively stained pellets from low speed centrifugation containing a mixture of Kelch and phalloidin-stabilized F-actin show loose bundling and cross-linking. Bar, 1 μm. (D) Bacterially expressed KREPs visualized with streptavidin-HRP. 0.25 μM of KREP four fails to cosediment with 0.5 μM of actin after centrifugation at 100,000 *g* (lanes 1 and 2). Increasing concentrations (0.25, 1, 2, 2.5, and 5 μM) of KREP five cosediment with actin in a saturable manner. (E) 0.5 μM of mutant KREPs mixed with 0.5 μM of actin. Repeat 5 cosediments with actin but not with 5 μM of the control protein BSA. Repeat 5 with an aspartate substituted at residue 627 (Y627D) fails to sediment with BSA control, and less than 50% of the protein sediments with actin (lanes 5–8). Similarly, repeat 5 with a glutamate in position 627 (Y627E) also fails to sediment with BSA and slightly less than 50% remains in the supernatant when sedimented with F-actin (lanes 9–12). Repeat 5 with an alanine substituted at residue 627 (Y627A) fails to sediment with BSA control and 100% of the protein sediments with actin (lanes 13–16). Similarly, repeat 5 with a phenylalanine in position 627 (Y627F) also fails to sediment with BSA and 100% sediments with F-actin (lanes 17–20).

cross-links in ring canals. The nonphosphorylatable mutant also caused a reduction in actin monomer turnover kinetics. This suggests that reversible cross-links are required to allow dynamic actin monomer turnover and maintain overall ring canal morphology. These observations suggest that a major cytoskeletal target of Src64 signaling at the ring canal is the actin–cross-linking protein Kelch.

Results

Kelch is phosphorylated and interacts with actin in a Src64-dependent manner

Based on motif searches (Hofmann et al., 1999), we determined that there were two predicted tyrosine phosphorylation sites in Kelch. The first was in the BTB dimerization domain at residue 132 (Fig. 1 A), and the second was within the fifth KREP at residue 627 (Fig. 1, A and B, shaded). The fifth KREP in α-scruin has been shown to bind F-actin (Sun et al., 1997). We performed site-directed mutagenesis to change the tyrosines to alanines, which are incapable of being phosphorylated. Transgenes encoding these constructs were designated *P[kelY132A]* and *P[kelY627A]*. At least three transgenic lines for each mutant were examined in a *kelch* mutant background (see Materials and methods for a detailed description of the genotypes tested).

To examine Kelch phosphorylation in the *Drosophila* ovary, we performed 2D electrophoresis of ovary lysates from several genetic backgrounds. When wild-type ovary lysates were treated with phosphatase inhibitors, a tyrosine-phosphorylated protein that comigrated with one of two Kelch isoforms was detected (Fig. 2, A, C, and H). Antibodies to phosphoserine and phosphothreonine showed no immunoreactivity comigrating with Kelch (unpublished data). Comparison to pH standards showed that the shift observed between the two Kelch isoforms was equivalent to the addition of a single phosphate. In the absence of phosphatase inhibitors, Kelch migrated as a single spot with no corresponding phosphotyrosine staining (Fig. 2, B and D). Egg chambers dissected from $src64^{\Delta 17}$ homozygous flies did not contain the phosphorylated form of Kelch (Fig. 2 E). In the presence of phosphatase inhibitors, Kelch protein from kel^{DE1};*P[kelY132A]*/+ ovaries continued to be tyrosine phosphorylated (Fig. 2 F). However, Kelch tyrosine phosphorylation in kel^{DE1};*P[kelY627A]*/+ ovaries was absent (Fig. 2 G). To characterize the effects of phosphorylation on the ability of Kelch to bind actin, we performed an actin overlay experiment. Total ovary lysates from wild-type ovaries were separated using 2D electrophoresis, and the blots were incubated with F-actin and then actin antibodies to detect bound actin. Only nonphosphorylated Kelch (KelY627A) bound actin (Fig. 2 I). To verify that actin binding was due to Kelch, we tested ovary lysates from a *kelch* mutant and determined that there was no longer actin binding present in the area where Kelch protein would have focused (unpublished data).

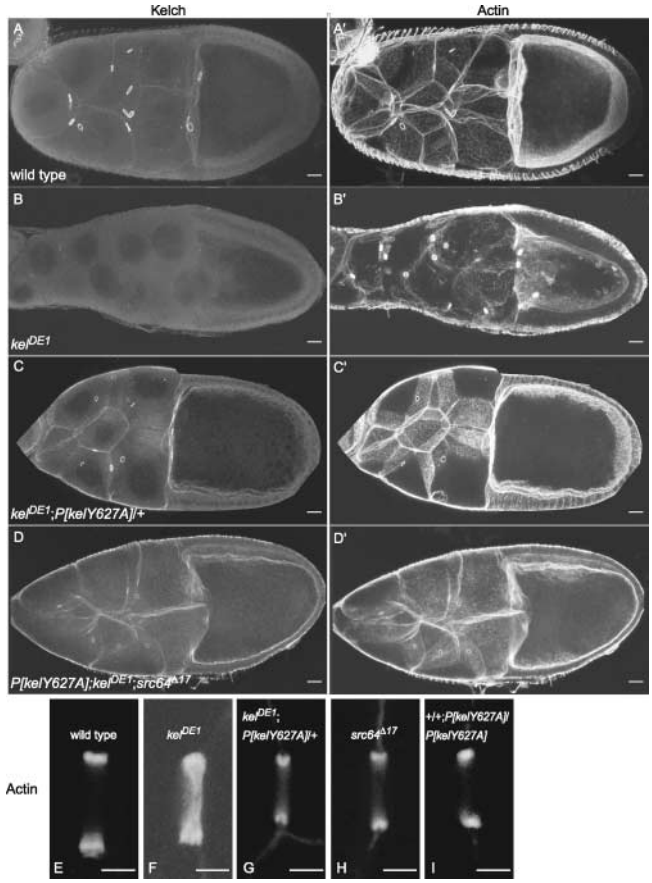

Figure 4. **Kelch and actin staining in stage 10A egg chambers.** (A) Wild-type egg chambers stained with anti-kelch antibody have a ring canal localization pattern. (A′) The rhodamine-phalloidin staining of this egg chamber shows the tight colocalization with the ring canal Kelch staining. (B) There is no Kelch staining present in the egg chambers made by females with the *kel^{DE1}* null mutation. (B′) Rhodamine-phalloidin staining of *kel^{DE1}* shows the massive disorganization of the ring canal actin characteristic in later stages of oogenesis. (C) Expression of KelY627A in a *kel^{DE1}* background shows that KelY627A protein properly localizes to the ring canal and is expressed at levels comparable to wild type. (C′) Actin staining in *kel^{DE1};P[kelY627A]/+* shows that ring canal F-actin organization is largely rescued. (D) Expression of KelY627A in a *kel^{DE1};src64$^{\Delta 17}$* background shows that KelY627A properly localizes to the ring canal and is expressed at levels comparable to wild type. (D′) Actin staining in *P[kelY627A];kel^{DE1};src64$^{\Delta 17}$* shows that ring canal F-actin organization is largely rescued and the overall phenotype is unchanged. (E) A horizontal section through wild-type ring canals exposes a typical actin rim. (F) A section through a *kel^{DE1}* ring canal shows that actin partially obstructs the ring canal lumen. (G) *kel^{DE1};P[kelY627A]/+* ring canal rims have a more concave appearance, similar to a bicycle rim. Also note that the ring canal diameter is significantly smaller than wild type. (H) A *src64$^{\Delta 17}$* ring canal has a shape very similar to *kel^{DE1};P[kelY627A]/+*. (I) Expression of two copies of *P[kelY627A]* in a wild-type background, *+/+; P[kelY627A]/P[kelY627A],* leads to a smaller diameter but not a notable disruption in the organization of the actin rim. Bars: (A–D) 20 μm; (E–I) 2 μm.

These results indicated that the tyrosine residue at position 627 was phosphorylated in a Src64-dependent manner, and phosphorylation of that residue disrupted Kelch binding to actin.

Kelch binds and cross-links F-actin via the fifth KREP

We tested the ability of purified recombinant Kelch protein to interact with F-actin. In preliminary experiments, the majority of Kelch sedimented in the presence of F-actin and remained in the supernatant in its absence (Fig. 3 A; and unpublished data). Saturation binding was determined by incubating purified Kelch with phalloidin-stabilized F-actin in increasing ratios, followed by 100,000 *g* centrifugation (Fig. 3 A). As the Kelch/actin ratio increased, more Kelch remained in the supernatant. The stoichiometry of Kelch binding to actin was estimated using a saturation curve in which the ratio of Kelch to actin in the pellet was plotted against increasing concentrations of Kelch (unpublished data). From this curve, the molar ratio of Kelch to F-actin was calculated as 1:4.

To determine if Kelch could cross-link F-actin, low speed sedimentation at 16,000 *g* was performed. When a saturating concentration of Kelch was added, most of the F-actin pelleted (unpublished data), suggesting that the actin was being cross-linked into bundles. Negative staining of F-actin, sedimented with or without Kelch, was performed to further determine the nature of the interaction. The actin-alone sample contained mainly single filaments (Fig. 3 B). In contrast, pellets from mixtures of Kelch and actin contained mostly loose bundles of actin filaments (Fig. 3 C). These observations suggested that full-length Kelch acted to bundle ring canal F-actin.

We mapped the F-actin binding domain to a single KREP by expressing and purifying each individual repeat and then performing high speed centrifugation in the presence of F-actin. KREPs 1–4 and 6 failed to cosediment with F-actin (Fig. 3 D, repeat 4, lanes 1 and 2). KREP five was capable of binding F-actin in a saturable manner (Fig. 3 D, lanes 3–12). To address the effect of phosphorylation, we introduced aspartate or glutamate residues at position 627 to mimic phosphorylation (Jordan and Karess, 1997; Waites et al., 2001). Both substitutions disrupted the ability of KREP five to bind F-actin, resulting in >50% of each mutant repeat remaining in the supernatant after high speed centrifugation (Fig. 3 E, lanes 7 and 11). To demonstrate that the substitution made in the KelY627A protein would not affect actin binding, we tested the substitution in vitro. Neither alanine nor phenylalanine substitutions disrupted actin binding (Fig. 3 E, lanes 13–20). These data suggest that F-actin binding by KREP five is likely to be reduced by phosphorylation of the tyrosine residue at position 627.

Characterization of KelY627A ring canal morphology

To study the role of Kelch phosphorylation in vivo, we examined *kelch* mutant flies expressing KelY627A protein in the germline. Wild-type stage 10A egg chambers stained with the Kel1B monoclonal antibody had a ring canal staining pattern that colocalized with F-actin (Fig. 4, A and A′). Egg chambers from *kelch* mutants showed a complete absence of Kelch protein staining (Fig. 4 B), and the well-characterized phenotype of ring canal actin disorganization with partial occlusion of the lumen (Tilney et al., 1996; Robinson and Cooley, 1997a) (Fig. 4 B′). The expression of one copy of *P[kelY627A]* in *kelch* mutants resulted in restoration of

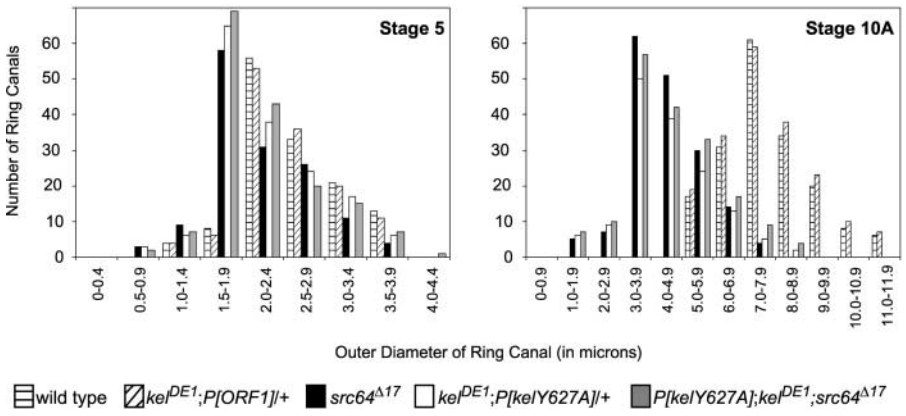

Figure 5. **Measurements of ring canal diameters in indicated genotypes using light microscopy.** (left) The distribution of ring canal diameters at stage 5 is similar in all genotypes. (right) At stage 10A, *src64*$^{\Delta 17}$ (solid bar), *kel*^{DE1};*P[kelY627A]*/+ (white bar), and *P[kelY627A];kel*^{DE1};*src64*$^{\Delta 17}$ (gray bar) ring canals are significantly ($P < 0.01$) smaller than wild-type ring canals (horizontal hatching), and *kelch* mutant ring canals rescued with a wild-type transgene, *kel*^{DE1};*P[ORF1]*/+ (diagonal hatching). The average wild-type ring canal diameter was 7–7.9 μm, whereas mutant ring canals were only 3–5 μm.

Kelch localization to ring canals and a rescue of F-actin organization (Fig. 4, C and C′), showing that the KelY627A protein had F-actin binding and cross-linking activity in vivo. The phenotype of KelY627A was not changed in a *src64*$^{\Delta 17}$ background (Fig. 4, D and D′). At a higher magnification, horizontal sections of wild-type ring canals were characterized by the appearance of two parallel rims of actin (Fig. 4 E). In *kelch* mutants, there was the typical collapse of actin into the lumen, almost completely obstructing the ring canal (Fig. 4 F). Comparison of wild type, *kel*^{DE1};*P[kelY627A]*/+, and *src64*$^{\Delta 17}$ revealed an increase in the concavity of the actin rim in both mutants, causing the appearance of a bicycle rim shape as well as a decrease in the diameter of the ring canal (Fig. 4, compare E, G, and H). These observations suggested that the phenotype in *kel*^{DE1};*P[kelY627A]* closely resembled *src64*$^{\Delta 17}$. Additionally, the introduction of two copies of *P[kelY627A]* into a wild-type background caused a decrease in ring canal diameter (Fig. 4 I). This dominant-negative phenotype indicated that the introduction of "irreversible" cross-links formed by KelY627A perturbed the function of endogenous Kelch.

Using light microscopy, we measured ring canal diameters in five backgrounds: wild type, *src64*$^{\Delta 17}$, kel^{DE1};*P[ORF1]*, *kel*^{DE1};*P[kelY627A],* and *P[kelY627A];kel*^{DE1};*src64*$^{\Delta 17}$ (see Materials and methods for details of each genotype). *P[ORF1]* is a transgene encoding wild-type Kelch protein that completely rescues the *kelch* phenotype (Robinson and Cooley, 1997b). The diameters of stage 5 ring canals in all the genotypes examined were similar with only a slight shift toward smaller rings in the three mutants (Fig. 5, stage 5). In contrast, the diameters of stage 10A wild-type and *kel*^{DE1};*P[ORF1]* ring canals were significantly larger than those of *kel*^{DE1};*P[kelY627A]*, *src64*$^{\Delta 17}$, and *P[kelY627A];kel*^{DE1};*src64*$^{\Delta 17}$ (Fig. 5, stage 10A). The distributions of *src64*$^{\Delta 17}$, *kel*^{DE1};*P[kelY627A]*, and *P[kelY627A];kel*^{DE1};*src64*$^{\Delta 17}$ diameters were identical, suggesting a common defect in ring canal morphogenesis.

Electron microscopy of ring canals during oogenesis

To better characterize the phenotype caused by KelY627A protein expression, we performed thin section electron microscopy on wild-type and mutant egg chambers. Horizontal sections cut through a ring canal reveal the two sides of the ring canal (diagramed in Fig. 6 A). Stage 6 ring canals from wild type, *kel*^{DE1};*P[kelY627A]*, and *src64*$^{\Delta 17}$ had roughly similar morphologies (Fig. 6, compare B–D); the plasma membranes forming the outer ring canal rim were perpendicular to the lumen with a continuous actin cytoskeleton making up the inner rim. However, late stage ring canals had distinct differences. In wild type, the continuous F-actin layer of ring canals transformed into separate actin cables (Fig. 6 E, arrows). This was accompanied by a remodeling of the electron-dense material located on the outer rim (Fig. 6 E, arrowheads) so that electron-dense material remained in apposition to the actin filaments. In both *kel*^{DE1};*P[kelY627A]* and *src64*$^{\Delta 17}$ mutants, the ring canal F-actin remained continuous with no separation into cables (Fig. 6, F and G). The electron-dense material of the outer rim also remained continuous, suggesting that the actin segregation shares a pathway with outer rim restructuring. Finally, there was a dramatic distortion of ring canal morphology resulting in a pointed rather than flat shape (Fig. 6, F and G). We concluded that the failure to resolve the F-actin rim into cables and the subsequent distortion of the underlying membrane caused the "bicycle rim" shape seen by light microscopy.

Using the thin section images, we measured several ring canal dimensions (Fig. 7 A) in wild type and *kel*^{DE1};*P[kelY627A]*. By stage 6, *kel*^{DE1};*P[kelY627A]* inner rim actin was 25–35% thicker than wild-type actin (Fig. 7 B). This significant difference ($P < 0.01$) in thickness remained roughly constant throughout ring canal growth. Although there was a significant decrease in *kel*^{DE1};*P[kelY627A]* ring canal diameter (Fig. 7 C), it was less than what was observed by light microscopy (Fig. 5, stage 10A). This discrepancy is probably due to the inherent difficulty of using serial thin sections to define the diameter of a circular ring canal. Wild-type and mutant ring canal lengths, measured by tracing the length of the outer rim, remained similar during ring canal growth (Fig. 7 D). Filament number per section (Fig. 7 A) increased by 50% in *kel*^{DE1};*P[kelY627A]* by stage 10A (Fig. 7 E). The density of actin filaments (Fig. 7 A) in wild type and *kel*^{DE1};*P[kelY627A]* was identical (Fig. 7 F). Therefore, although there were comparable densities of actin filaments in wild type and *kel*^{DE1};*P[kelY627A]*, the failure to form actin cables in *kel*^{DE1};*P[kelY627A]* led to a significant increase in the total amount of actin present in each section.

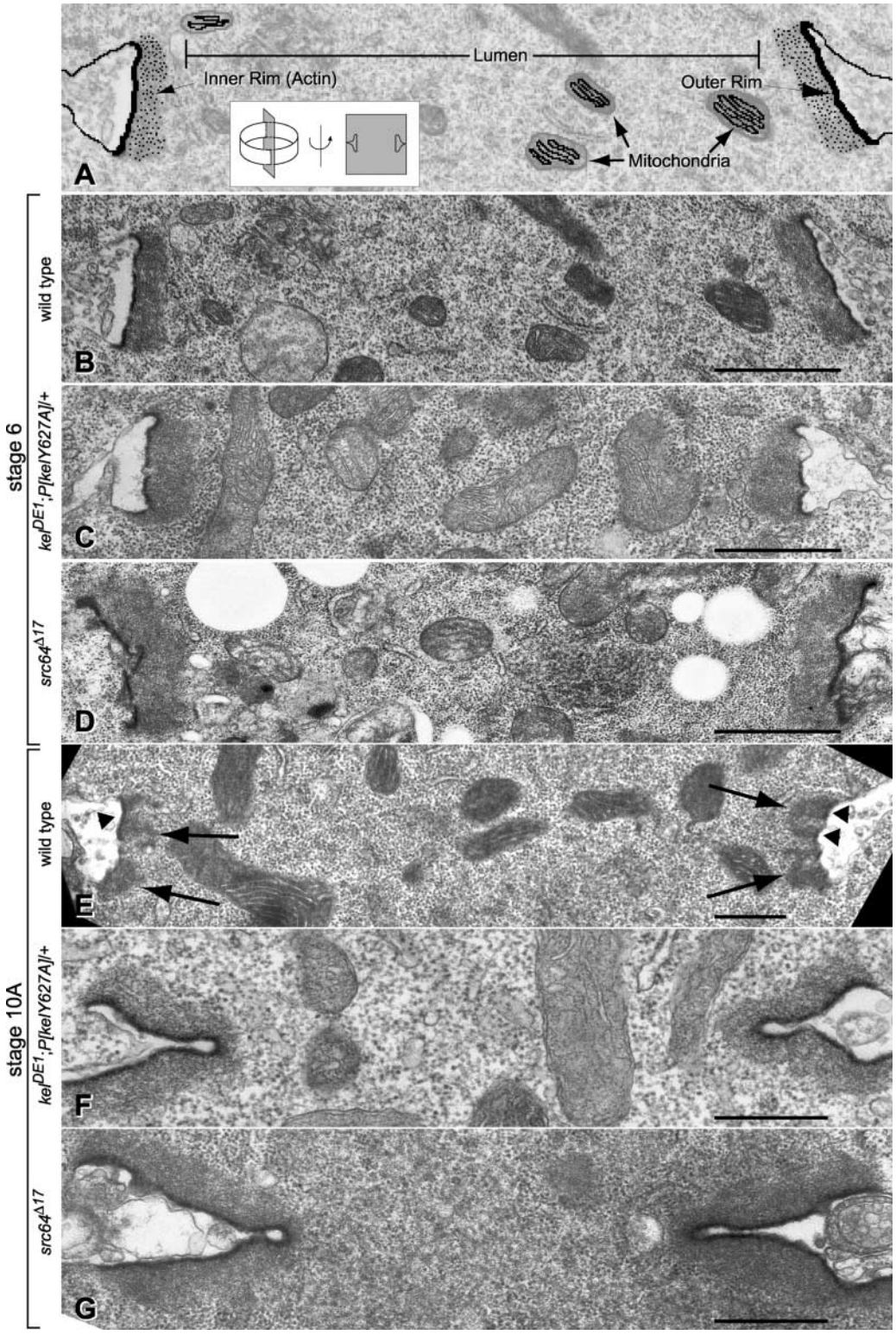

Figure 6. **Thin section electron micrographs of ring canals.** (A) A schematic illustrating the components visualized in a vertical section of a ring canal (see inset). The inner rim is rich in F-actin (dots), whereas the electron-dense material forming the outer rim is continuous with the plasma membrane. The lumen of the ring canal rim is large enough for mitochondria to pass through. (B) Wild-type stage 6 ring canals have a tightly organized band of actin evenly distributed across the length of the outer rim. (C) *kel*^{DE1};*P[kelY627A]*/+ mutant ring canals have a slightly thicker actin band at stage 6 (see Fig. 7 for quantitation). (D) *src64*$^{\Delta 17}$ mutant ring canals also have thicker actin at stage 6. (E) Wild-type stage 10A ring canals have separated actin cables (arrows). This separation is mirrored in the rearrangement of the electron-dense outer rim (arrowheads). (F) *kel*^{DE1};*P[kelY627A]*/+ ring canals do not exhibit the same segregation of actin into cables. Moreover there is no fragmentation of the outer rim, and it instead folds into a pointed shape. (G) *src64*$^{\Delta 17}$ ring canals phenocopy *kel*^{DE1};*P[kelY627A]*/+ at stage 10A. Bars,1 μm.

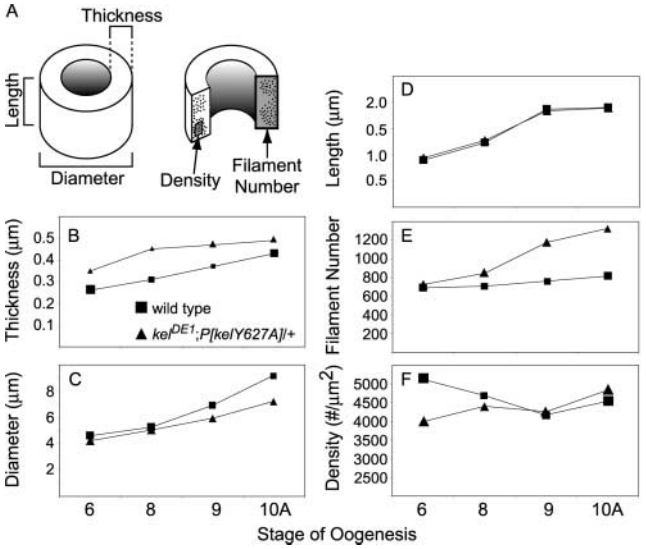

Figure 7. **Quantitation of thin-section electron micrograph data.** Wild-type (■) and *kel*^{DE1};*P[kelY627A]*/+ (▲) ring canals are compared over four stages of development (6, 8, 9, and 10A). At least seven ring canals were measured at each stage. (A) A ring canal can be characterized as a tube with three dimensions: length, diameter (to the outer rim), and thickness of the inner rim. Counting the total number of actin filaments per ring canal section leads to the filament number. The density of actin filaments was calculated by counting filaments in 10 nm^2 segments of the inner rim that contained actin. (B) Beginning at stage 6 of oogenesis, there is a statistically significant increase ($P < 0.01$) in inner rim thickness in *kel*^{DE1};*P[kelY627A]*/+ compared with wild type. (C) Beginning at stage 9, *kel*^{DE1};*P[kelY627A]*/+ ring canal diameters are smaller than wild type. (D) The lengths of the outer rims are similar during all observed stages. (E) Actin filament number increases in *kel*^{DE1};*P[kelY627A]*/+, and by stage 10A there are nearly 50% more filaments per section compared with wild type. (F) Although there may be an initial difference in actin density, wild-type and *kel*^{DE1};*P[kelY627A]*/+ ring canals ultimately have similar actin densities (measurements of wild-type stages 8 and 10A are from Tilney et al., 1996). The size of each data point represents the standard error of measurement.

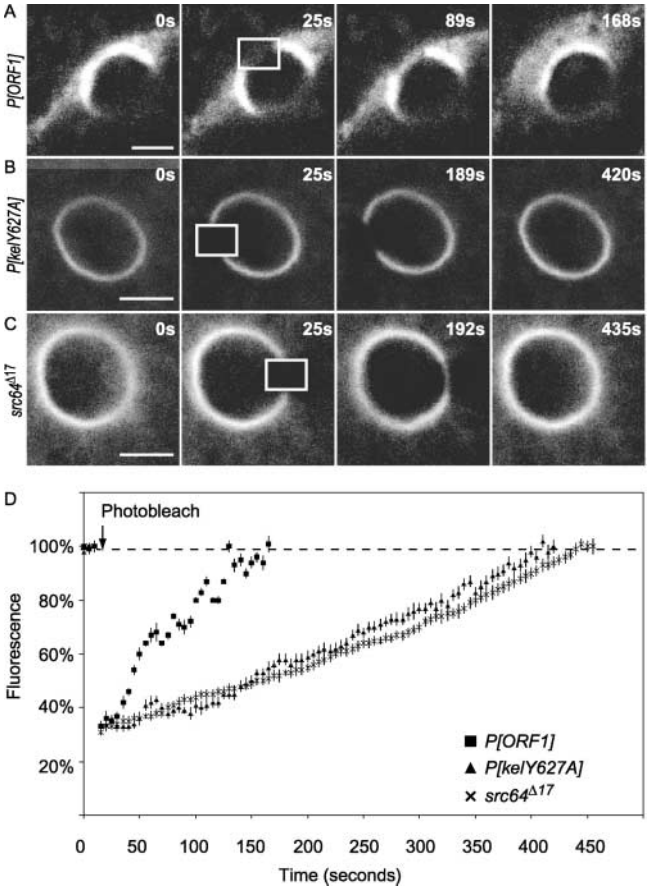

Figure 8. **Photobleaching reveals reduced monomer exchange in KelY627A and *src64*$^{\Delta 17}$ ring canals.** FRAP experiments with GFP–actin were used to measure actin dynamics in *kelch* mutant ring canals, containing either wild-type (*P[ORF1]*) or mutant (*P[kelY627A]*) rescuing transgenes, and in *src64*$^{\Delta 17}$. (A) A representative time series of FRAP in a ring canal expressing wild-type Kelch (*P[ORF1]*). The box outlined at 25 s represents the area photobleached by the laser. By 168 s, all of the fluorescence had returned. (B) A similar time series of FRAP in a ring canal expressing nonphosphorylatable Kelch (*P[kelY627A]*). The area bleached at 25 s took 420 s to recover. (C) A FRAP assay of *src64*$^{\Delta 17}$, where the area bleached at 25 s took 435 s to recover. Bars, 5 μm. (D) A graph representing FRAP of 21 *P[ORF1]* (■), 23 *P[kelY627A]* (▲), and 15 *src64*$^{\Delta 17}$ (×) stage 10A ring canals with error bars representing the standard deviation. *P[kelY627A]* and *src64*$^{\Delta 17}$ ring canals take more than three times as long to recover to prebleach levels as *P[ORF1]* ring canals.

Actin monomer exchange decreases in KelY627A

To further characterize the phenotype caused by KelY627A protein, we performed the fluorescence recovery after photobleaching (FRAP) assay using actin tagged with green fluorescent protein (GFP–actin). The expression of GFP–actin was driven by a germline-specific promoter to label ring canals throughout all stages of development. FRAP was measured in stage 10A egg chambers from transgenic flies expressing wild-type Kelch (ORF1) and KelY627A. 18 *P[UAS-GFP–Actin]*/*P[ORF1]*, 21 *P[UAS-GFP–Actin]*/*P[kelY627A]*, and 15 *P[UAS-GFP–Actin]*;*src64*$^{\Delta 17}$ ring canals were analyzed. Three representative experiments are shown (Fig. 8, A–C). After bleaching, ring canals in *P[UAS-GFP–Actin]*/*P[ORF1]* recovered fluorescence with a $t_{1/2}$ of 65 s (Fig. 8 D). In contrast, fluorescence in *P[UAS-GFP–Actin]*/*P[kelY627A]* ring canals recovered with a $t_{1/2}$ of 227 s (Fig. 8 D). *P[UAS-GFP–Actin]*;*src64*$^{\Delta 17}$ had a $t_{1/2}$ of 244 s. These data indicate that in ring canals with nonphosphorylatable Kelch or reduced Src64, actin monomers took >3.5 times as long to exchange as in control ring canals.

Discussion

We have shown that *Drosophila* Kelch protein is an actin filament–cross-linking protein essential for the organization of actin in ovarian ring canals. F-actin binding by Kelch is negatively regulated by phosphorylation of the tyrosine residue at position 627, which is within the fifth KREP. Because KREP five contains the actin binding site, the addition of a phosphate is likely to sterically interfere with actin filament binding as has been found for other actin-binding proteins, villin (Zhai et al., 2001) and α-actinin (Izaguirre et al.,

2001). Phosphorylation of Kelch tyrosine 627 depends directly or indirectly on the Src64 kinase, and the expression of a nonphosphorylatable Kelch protein phenocopies *src64* mutations. Additionally, actin has reduced exchange rates in the ring canal as measured by FRAP using GFP–actin. These data suggest that Kelch may be the primary, if not only, cytoskeletal target of Src64-dependent kinase activity in ring canals, and the regulated cross-linking of Kelch plays a role in the remodeling of actin during ring canal growth.

Regulation of ring canal expansion

The dynamics of actin filaments in ring canals have been elegantly described at the ultrastructural level (Riparbelli and Callaini, 1995; Tilney et al., 1996). Ring canals are built at the positions of arrested cleavage furrows that form during the mitotic divisions of germline cells. The mechanism of cleavage furrow arrest is likely to be conserved among animal species because incomplete cytokinesis occurs during the proliferation of germline cells in many animals (for review see Robinson and Cooley, 1996). In *Drosophila*, once egg chambers are fully assembled, ring canal growth happens in two phases. First, the thickness of the actin rim increases to ~0.3 μm as the diameter of the ring grows slowly to 2 μm. Subsequently, the thickness of the actin rim and the density of actin filaments remain constant while the rate of ring canal expansion increases. The net increase of actin within ring canals overall is 134-fold (Tilney et al., 1996). During the rapid phase of ring canal growth, actin filaments must be polymerized, probably at the plasma membrane, to expand the ring canal rim, and disassembled at the cytoplasmic face to maintain the lumen. Our analysis of the Kelch protein shows that precise regulation of actin filament cross-linking by phosphorylation is critical during rapid ring canal growth.

The behavior of ring canals that contain KelY627A provide significant insight into Kelch function. The absence of Kelch phosphorylation leads to ring canals that accumulate more actin filaments than normal, possibly due to a slowing in the rate of actin depolymerization relative to the rate of polymerization. After about stage 8 of oogenesis, the failure to resolve the continuous sheet of actin filaments into discreet cables may be another consequence of inhibiting depolymerization. The presence of more "permanent" Kelch cross-links may reduce the accessibility of the filament network to depolymerizing factors. In vitro experiments have demonstrated that actin–cross-linking proteins alone are capable of inhibiting the rate of pyrenyl F-actin depolymerization (Cano et al., 1992). Another possible explanation for these phenotypes is that because Kelch cross-links are no longer easily reversible, filament reorientation or sliding is restricted during ring canal growth.

The FRAP experiments provide additional insight into the actin dynamics at the ring canal. First, ring canal actin is highly dynamic. The rate of actin monomer turnover that we found in wild-type ring canals is comparable to the kinetics of actin turnover found in the leading edge of motile goldfish epithelial keratocytes (Theriot and Mitchison, 1991). This would be consistent with a population of actin that is constantly undergoing a rapid cycle of polymerization and depolymerization. Second, the presence of nonregulated Kelch clearly results in a dramatic reduction in the dynamics of actin. This supports the model that mutant Kelch protein reduces accessibility to other actin-binding proteins, in this case proteins involved with polymerization or depolymerization. We propose that this effect could be due to bound Kelch acting as a stabilizing protein much in the same way that tropomyosin protects F-actin from actin depolymerizing factor/cofilin (for review see Pollard et al., 2000).

Studies in our lab involving the actin polymerization factor Arp2/3 have demonstrated that ring canal stability and growth is dependent on the presence of a functional Arp2/3 complex (Hudson and Cooley, 2002). The effects of mutations in Arp2/3 complex subunits are progressively more severe as egg chambers develop, and by stage 6, ring canals begin to collapse. In *kelch* null mutants, the actin filaments are initially well organized, begin to show signs of disorganization around stage 4, and are completely disorganized starting at stage 6 (Tilney et al., 1996; Robinson and Cooley, 1997a). Interestingly, thin section electron micrographs of kel^{DE1}; *P[kelY627A]/+* show signs of actin filament disruption beginning at stage 6. The coincidence of *kelch* and Arp2/3 complex mutant phenotypes with the onset of rapid ring canal expansion and the presence of highly dynamic actin, suggest a model where ring canal growth is powered by de novo actin polymerization accompanied by regulated cross-links. Therefore, ring canal growth may be mechanistically similar to the movement of plasma membranes at the leading edge of motile cells. Future work on ring canal actin organization should include platinum replica electron microscopy to understand the overall organization of the ring canal actin filament network. This will allow direct comparison to the actin filament networks of lamellipodia in *Xenopus laevis* keratocytes and fibroblasts (Svitkina and Borisy, 1999).

Intriguingly, the accumulation of actin during earlier stages of oogenesis is apparently independent of both Kelch and the Arp2/3 complex. Characterization of other mutants affecting ring canals has revealed genes required for initial stages of ring canal assembly. These include the *cheerio* gene that encodes the actin filament–cross-linking protein ABP280/filamin (Li et al., 1999; Sokol and Cooley, 1999). In *cheerio* mutants, ring canal actin is absent. In addition, HtsRC is required for the early accumulation of actin filaments (Robinson et al., 1994); however, it has not been determined whether HtsRC interacts directly with F-actin or affects actin polymerization. Therefore, additional research is needed to elucidate the mechanism of early ring canal biogenesis.

The regulation of Kelch–actin cross-links could be accomplished by Src64 directly phosphorylating Kelch. Alternatively, Src64 may activate another protein tyrosine kinase, such as Tec29 (Roulier et al., 1998), which in turn phosphorylates Kelch. However, the shared phenotype seen by electron microscopy of the *src64* and *P[kelY627A]* ring canals is strongly suggestive of Kelch being the major downstream component of a Src64 cascade. Analysis of Kelch phosphorylation in *tec29* mutants is difficult because available *tec29* alleles are lethal. SFKs have been shown to signal rearrangements in the actin cytoskeleton in other contexts. In *Drosophila*, embryos mutant for *src64* or *tec29* fail to complete epidermal closure at the end of gastrulation. This is, in part, because the leading edge cells contain reduced quantities of F-actin, and the cells only partially elongate and fail to migrate completely

(Tateno et al., 2000). SFKs are also known to interact directly with cytoskeletal proteins, as in the case of c-Src and cortactin. Phosphorylation of cortactin by c-Src tyrosine kinase decreases its ability to cross-link F-actin in vitro (Bourguignon et al., 2001). These examples suggest that there could be a critical role played by tyrosine phosphatases to ensure that F-actin does not become disorganized due to excessive phosphorylation of cross-linking proteins. There are several candidate phosphatases in *Drosophila*; however, their roles in ring canal development have not been studied.

Kelch family members and actin

It should be noted that not all Kelch family members are actin-binding proteins (for review see Adams et al., 2000). For example, nuclear restricted protein/brain (NRP/B) is a novel nuclear matrix protein that contains a highly conserved KREP domain. NRP/B is specifically expressed in primary neurons and participates in the regulation of neuronal process formation (Kim et al., 1999). A direct interaction with actin by the ectoderm neural cortex-1 protein has been demonstrated by coimmunoprecipitation; however, it does not exclusively colocalize with F-actin in Daoy cells, and it is perinuclear in neuronal cell lines (Hernandez et al., 1997).

A Kelch family member that interacts with actin is called Mayven. Mayven localizes to the leading edge of the lamellipodia in U373-MG astrocytoma/glioblastoma cells (Soltysik-Espanola et al., 1999). Mayven is also localized with the focal adhesion kinase (Soltysik-Espanola et al., 1999), suggesting it could play a role in actin reorganization at focal adhesion plaques. A role for phosphorylation in the regulation of Mayven has not been reported.

In *Limulus*, it has been postulated that the Kelch homologue α-scruin acts as a protein that allows F-actin to rapidly twist and slide during acrosome extension or "true discharge" (Sherman et al., 1999). Biochemical studies performed on α-scruin (Sun et al., 1997) have shown that the cysteine corresponding to *Drosophila* Kelch residue 628 lies within the α-scruin actin binding domain (Fig. 2 B, boxed). Thus, both Kelch and α-scruin contain an actin binding site within KREP number 5. However, α-scruin does not have a tyrosine comparable to Kelch residue 627 in the primary sequence; therefore, regulation of α-scruin cross-linking is likely to be different than that for Kelch. α-Scruin regulation may target scruin–scruin interactions rather than scruin–actin interactions.

Materials and methods

Drosophila stocks and germline transformation

w^{1118} (Lindsley and Zimm, 1992), $src64^{\Delta 17}$ (Guarnieri et al., 1998; obtained from S. Beckendorf, University of California, Berkeley, CA), kel^{neo} (Xue and Cooley, 1993; Robinson and Cooley, 1997b), and kel^{DE1} (Schüpbach and Wieschaus, 1991) were maintained under standard culturing conditions. Mutants for transgenic studies were generated using PCR amplification, sequenced to confirm that there were no PCR-induced errors, and then subcloned into the germline expression vector pCOG (Robinson and Cooley, 1997b). Mutant constructs were microinjected along with the Δ2-3 transposase helper plasmid into w^{1118} syncytial blastoderm embryos according to standard techniques. P-element insertions were maintained in a w^{1118} background, as well as in kel^{neo} and kel^{DE1} backgrounds.

The GFP–actin fusion construct was made by subcloning the EcoRI/NotI GFP–actin fragment from pUAST-GFP–actin (Verkhusha et al., 1999) into pBluescript II KS(−). The 1.9-kb KpnI/NotI fragment from pBluescript was subcloned into pUASp2, a modified pUASp (Rorth, 1998).

GFP–actin was then expressed in the ovary using nanos-Gal4-VP16 (Van Doren et al., 1998). The three genotypes used for FRAP assays were (1) *P[UAS-GFP–Actin]/P[ORF1]*: w^{1118};kel^{DE1},$P[w^+$ *nos-Gal4-vp16]*/kel^{DE1}; *P*[w^+ *ORF1]*/*P*[w^+ *UASp2-GFP–actin]*; (2) *P[UAS-GFP–Actin]/P[kelY627A]*: w^{1118};kel^{DE1},$P[w^+$ *nos-Gal4-vp16]*/kel^{DE1};*P*[w^+ *kelY627A]*/*P*[w^+ *UASp2-GFP–actin]*; and (3) *P[UAS-GFP–Actin]/*$src64^{\Delta 17}$: w^{1118};*P*[w^+ *nos-Gal4-vp16]*/*P*[w^+ *UASp2-GFP–actin]*;$src64^{\Delta 17}$/$src64^{\Delta 17}$.

Electron microscope procedures

Egg chambers were dissected into IMADS (100 mM sodium glutamate, 25 mM KCl, 15 mM $MgCl_2$, 5 mM $CaSO_4$, and 2 mM sodium phosphate buffer, pH 6.9) (Singleton and Woodruff, 1994). Egg chambers were then fixed, stained, and embedded as previously described (Tilney et al., 1996). Detergent extraction and actin quantitation of ring canals were performed as previously described (Tilney et al., 1996). Negative staining of actin and Kelch mixtures was performed as previously described (Harris, 1999). Electron microscopy was performed on a Phillips Tecnai electron microscope at an accelerating voltage of 80 kV. Wild-type and mutant ring canal dimensions were compared using the *t* test, and a *P* value of <0.01 was taken as significant. The *t* test was performed using Microsoft Excel 2000.

Protein purification

Full-length Kelch and individual KREP constructs were made using amino acid numbers corresponding to the sequence in Xue and Cooley (1993). ORF1, the full-length Kelch cDNA (Robinson and Cooley, 1997a), was modified using PCR to introduce HindIII and NotI restriction enzyme sites at the 5′ and 3′ ends. The following individual KREPs were generated: repeat 1 (L405-K450), repeat 2 (V451-C497), repeat 3 (I498-L544), repeat 4 (L545-I593), repeat 5 (L594-L640), repeat 5 (L594-[Y627D]-L640), repeat 5 (L594-[Y627E]-L640), repeat 5 (L594-[Y627A]-L640), repeat 5 (L594-[Y627F]-L640), and repeat 6 (L641-M689). The PCR products were cloned into pCR 2.1-TOPO according to the manufacturer's instructions (Invitrogen). The constructs were sequenced and subcloned into the PinPoint Xa-3 vector (Promega) using HindIII and NotI. *Escherichia coli* DH5α cells were transformed with the PinPoint Xa-3 Kelch constructs. Soluble Kelch and KREP fragments were obtained by following the manufacturer's instructions. Only full-length Kelch constructs were cleaved from the purification tag using Factor Xa and the manufacturer's instructions.

Image acquisition and FRAP

GFP-actin–expressing ovaries were dissected onto a 22-mm × 40-mm glass coverslip as previously described (Theurkauf and Hazelrigg, 1998). FRAP experiments were conducted on a Zeiss 510 scanning laser microscope (Center for Cell Imaging, Yale University, New Haven, CT). Images were captured with either a 63× 1.4 NA objective or a 40× 1.3 NA objective using a pinhole diameter equivalent to one to two times the Airy disk diameter. In each experiment, at least 20 consecutive baseline images were obtained before bleaching. A region of the ring canal was selected, and fluorescence was bleached by scanning the region with high intensity illumination (100% transmittance). After photobleaching, fluorescence of the entire field was collected by the ArKr laser at 1% power every second for at least 4 min after photobleaching. The fluorescence intensity in the photobleached region of the ring canal was normalized to the fluorescence measured in a nonbleached region of the same ring canal, and in the cytoplasm. Wild-type and mutant rate constants of three curves were compared, and a *P* value of <0.01 was taken as significant. Nonlinear regression and *t* tests were performed using Microsoft Excel 2000. Images were prepared for publication using Adobe Photoshop.

Protein electrophoresis and Western blot analysis

Ovaries were dissected in the presence or absence of 25 mM sodium vanadate, 10 mM sodium fluoride, and 0.05% hydrogen peroxide in IMADS buffer and incubated on ice for 5 min. 10 ovaries were then solubilized with 25 μl isoelectric focusing sample buffer (8 M urea, 4% [wt/vol] CHAPS, 40 mM Tris, 65 mM DTE, and a trace of bromophenol blue). Samples were focused using Immobiline Drystrips, pH 4–7 linear (Amersham Pharmacia Biotech). The second dimension was performed using standard SDS-PAGE techniques on 8% gels and transferred onto nitrocellulose membranes (Hybond ECL; Amersham Pharmacia Biotech). Membranes were blocked with PBS containing 5% nonfat dry milk and incubated with the following antibodies and dilutions: 1:10 anti-kelch 1B (Xue and Cooley, 1993), 1:10 anti-actin JLA20 (Developmental Studies Hybridoma Bank, University of Iowa, Iowa City, IA), and 1:2,000 anti-phosphotyrosine PY20 (ICN Biomedicals); and detection of biotin-labeled Kelch proteins was performed using a 1:5,000 dilution of avidin-HRP (Pierce Chemical Co.). Secondary antibodies conjugated with HRP were purchased from

Pierce Chemical Co. Visualization of HRP was performed using an ECL detection kit (Amersham Pharmacia Biotech).

Egg chamber staining

Ovaries were dissected, fixed, and processed as previously described (Robinson and Cooley, 1997a). For filamentous actin staining, egg chambers were incubated in 5 U of rhodamine-conjugated phalloidin (Molecular Probes) per 200 μl of PBTO (1 × PBS, 0.3% Triton X-100, 0.5% BSA). For antibody staining, ovaries were immunostained with anti-kelch 1B at a 1:1 dilution (Xue and Cooley, 1993), or anti-phosphotyrosine PY20 (ICN Biomedicals) at a 1:500 dilution. Secondary antibodies conjugated with Alexa Fluor 488 were purchased from Molecular Probes. Fluorescence intensity measurements were collected using the ZEISS image analysis software.

F-actin binding assays

Purified rabbit skeletal muscle monomeric actin was purchased from Cytoskeleton Inc. Actin concentration was estimated as previously described (Pollard, 1976). The concentration of Kelch and KREPs was determined using a modified Bradford assay (Bio-Rad Laboratories). G-actin was polymerized in A′ buffer (10 mM imidazole, pH 7.0, 75 mM KCl, 2.5 mM $MgSO_4$, 1 mM EGTA, 1 mM ATP, 0.1% NaN_3). Immediately before use, purified Kelch or KREPs and actin were centrifuged at 100,000 *g* at 4°C for 1 h to pellet any aggregated protein. Mixtures of F-actin with Kelch or KREPs were incubated for 10 min at 25°C. Low speed and high speed cosedimentation assays were performed as previously described (Matova et al., 1999).

Far Western blot analysis

For binding experiments, total ovary lysates were separated using 2D electrophoresis as described above. Nitrocellulose blots were incubated at 4°C overnight in in PBS containing 5% milk and 0.1% Tween 20, followed by incubation with 10 mg of F-actin (Sigma-Aldrich) for 2 h at 4°C. The blots were washed, and a 1:10 dilution of rabbit anti-actin antibody JLA20 was added for 1 h. After washing, HRP-conjugated anti–rabbit antibody (Pierce Chemical Co.) was added for 1 h. Bands were visualized using ECL reagents.

We would like to thank Dr. Marc Pypaert and Kimberly Zichichi for help with the Philips electron microscope, Dr. Michael H. Nathanson and Philippe Male at the Center for Cell Imaging for their help and technical advice, and Dr. Mark Mooseker for technical advice and critical discussion. We would also like to thank current and former members of the Cooley lab who have donated time to the discussion and thorough reading of this manuscript.

This research was supported by National Institutes of Health grant GM52702 to L. Cooley.

Submitted: 11 October 2001
Revised: 13 December 2001
Accepted: 14 January 2002

References

Adams, J., R. Kelso, and L. Cooley. 2000. The kelch repeat superfamily of proteins: propellers of cell function. *Trends Cell Biol.* 10:17–24.

Ahmad, K.F., C.K. Engel, and G.G. Prive. 1998. Crystal structure of the BTB domain from PLZF. *Proc. Natl. Acad. Sci. USA.* 95:12123–12128.

Bork, P., and R.F. Doolittle. 1994. *Drosophila* kelch motif is derived from a common enzyme fold. *J. Mol. Biol.* 236:1277–1282.

Bourguignon, L.Y., H. Zhu, L. Shao, and Y.W. Chen. 2001. CD44 interaction with c-Src kinase promotes cortactin-mediated cytoskeleton function and hyaluronic acid-dependent ovarian tumor cell migration. *J. Biol. Chem.* 276: 7327–7336.

Boyce, B.F., T. Yoneda, C. Lowe, P. Soriano, and G.R. Mundy. 1992. Requirement of pp60c-src expression for osteoclasts to form ruffled borders and resorb bone in mice. *J. Clin. Invest.* 90:1622–1627.

Brown, M.T., and J.A. Cooper. 1996. Regulation, substrates and functions of *src*. *Biochim. Biophys. Acta.* 1287:121–149.

Bullitt, E.S., D.J. DeRosier, L.M. Coluccio, and L.G. Tilney. 1988. Three-dimensional reconstruction of an actin bundle. *J. Cell Biol.* 107:597–611.

Cano, M.L., L. Cassimeris, M. Fechheimer, and S.H. Zigmond. 1992. Mechanisms responsible for F-actin stabilization after lysis of polymorphonuclear leukocytes. *J. Cell Biol.* 116:1123–1134.

Condeelis, J. 2001. How is actin polymerization nucleated in vivo? *Trends Cell Biol.* 11:288–293.

Dodson, G.S., D.J. Guarnieri, and M.A. Simon. 1998. Src64 is required for ovarian ring canal morphogenesis during *Drosophila* oogenesis. *Development.* 125:2883–2892.

Guarnieri, D.J., G.S. Dodson, and M.A. Simon. 1998. SRC64 regulates the localization of a Tec-family kinase required for *Drosophila* ring canal growth. *Mol. Cell.* 1:831–840.

Harris, J.R. 1999. Negative staining of thinly spread biological particulates. *In* Electron Microscopy Methods and Protocols. Vol. 117. M.A. Nasser Hajibagheri, editor. Humana Press, Totowa, NJ. 13–30.

Hernandez, M.C., P.J. Andres-Barquin, S. Martinez, A. Bulfone, J.L. Rubenstein, and M.A. Israel. 1997. ENC-1: a novel mammalian kelch-related gene specifically expressed in the nervous system encodes an actin-binding protein. *J. Neurosci.* 17:3038–3051.

Hofmann, K., P. Bucher, L. Falquet, and A. Bairoch. 1999. The PROSITE database, its status in 1999. *Nucleic Acids Res.* 27:215–219.

Hudson, A.M., and L. Cooley. 2002. A subset of dynamic actin rearrangements in *Drosophila* requires the ARP2/3 complex. *J. Cell Biol.* 156:677–687.

Izaguirre, G., L. Aguirre, Y.P. Hu, H.Y. Lee, D.D. Schlaepfer, B.J. Aneskievich, and B. Haimovich. 2001. The cytoskeletal/non-muscle isoform of alpha-actinin is phosphorylated on its actin-binding domain by the focal adhesion kinase. *J. Biol. Chem.* 276:28676–28685.

Jordan, P., and R. Karess. 1997. Myosin light chain–activating phosphorylation sites are required for oogenesis in *Drosophila*. *J. Cell Biol.* 139:1805–1819.

Kim, I.F., E. Mohammadi, and R.C. Huang. 1999. Isolation and characterization of IPP, a novel human gene encoding an actin-binding, kelch-like protein. *Gene.* 228:73–83.

Koch, E.A., and R.C. King. 1969. Further studies on the ring canal system of the ovarian cystocytes of *Drosophila melanogaster*. *Z. Zellforsch. Mikrosk. Anat.* 102:129–152.

Kramerova, I.A., and A.A. Kramerov. 1999. Mucinoprotein is a universal constituent of stable intercellular bridges in *Drosophila melanogaster* germ line and somatic cells. *Dev. Dyn.* 216:349–360.

Li, M.G., M. Serr, K. Edwards, S. Ludmann, D. Yamamoto, L.G. Tilney, C.M. Field, and T.S. Hays. 1999. Filamin is required for ring canal assembly and actin organization during *Drosophila* oogenesis. *J. Cell Biol.* 146:1061–1074.

Lindsley, D.L., and G.G. Zimm. 1992. The Genome of *Drosophila melanogaster*. Academic Press, San Diego. 1,133 pp.

Matova, N., S. Mahajan-Miklos, M.S. Mooseker, and L. Cooley. 1999. *Drosophila* quail, a villin-related protein, bundles actin filaments in apoptotic nurse cells. *Development.* 126:5645–5657.

Noegel, A.A., and M. Schleicher. 2000. The actin cytoskeleton of *Dictyostelium*: a story told by mutants. *J. Cell Sci.* 113:759–766.

Pantaloni, D., C. Le Clainche, and M.F. Carlier. 2001. Mechanism of actin-based motility. *Science.* 292:1502–1506.

Pollard, T. 1976. The role of actin in the temperature-dependent gelation and contraction of extracts of *Acanthamoeba*. *J. Cell Biol.* 68:579–601.

Pollard, T.D., L. Blanchoin, and R.D. Mullins. 2000. Molecular mechanisms controlling actin filament dynamics in nonmuscle cells. *Annu. Rev. Biophys. Biomol. Struct.* 29:545–576.

Pruyne, D., and A. Bretscher. 2000. Polarization of cell growth in yeast. *J. Cell Sci.* 113:571–585.

Riparbelli, M.G., and G. Callaini. 1995. Cytoskeleton of the *Drosophila* egg chamber: new observations on microfilament distribution during oocyte growth. *Cell Motil. Cytoskeleton.* 31:298–306.

Robinson, D.N., and L. Cooley. 1996. Stable intercellular bridges in development: the cytoskeleton lining the tunnel. *Trends Cell Biol.* 6:474–479.

Robinson, D.N., and L. Cooley. 1997a. *Drosophila* kelch is an oligomeric ring canal actin organizer. *J. Cell Biol.* 138:799–810.

Robinson, D.N., and L. Cooley. 1997b. Examination of the function of two kelch proteins generated by stop codon suppression. *Development.* 124:1405–1417.

Robinson, D.N., K. Cant, and L. Cooley. 1994. Morphogenesis of *Drosophila* ovarian ring canals. *Development.* 120:2015–2025.

Rorth, P. 1998. Gal4 in the *Drosophila* female germline. *Mech. Dev.* 78:113–118.

Roulier, E.M., S. Panzer, and S.K. Beckendorf. 1998. The Tec29 tyrosine kinase is required during *Drosophila* embryogenesis and interacts with Src64 in ring canal development. *Mol. Cell.* 1:819–829.

Sanders, M.C., M. Way, J. Sakai, and P. Matsudaira. 1996. Characterization of the actin cross-linking properties of the scruin-calmodulin complex from the

acrosomal process of *Limulus* sperm. *J. Biol. Chem.* 271:2651–2657.

Schüpbach, T., and E. Wieschaus. 1991. Female sterile mutations on the second chromosome of *Drosophila melanogaster.* II. Mutations blocking oogenesis or altering egg morphology. *Genetics.* 129:1119–1136.

Schwartzberg, P.L., L. Xing, O. Hoffmann, C.A. Lowell, L. Garrett, B.F. Boyce, and H.E. Varmus. 1997. Rescue of osteoclast function by transgenic expression of kinase-deficient Src in *src*−/− mutant mice. *Genes Dev.* 11:2835–2844.

Sherman, M.B., J. Jakana, S. Sun, P. Matsudaira, W. Chiu, and M.F. Schmid. 1999. The three-dimensional structure of the *Limulus* acrosomal process: a dynamic actin bundle. *J. Mol. Biol.* 294:139–149.

Singleton, K., and R.I. Woodruff. 1994. The osmolarity of adult *Drosophila* hemolymph and its effect on oocyte-nurse cell electrical polarity. *Dev. Biol.* 161:154–167.

Sokol, N.S., and L. Cooley. 1999. *Drosophila* filamin encoded by the *cheerio* locus is a component of ovarian ring canals. *Curr. Biol.* 9:1221–1230.

Soltysik-Espanola, M., R.A. Rogers, S. Jiang, T.A. Kim, R. Gaedigk, R.A. White, H. Avraham, and S. Avraham. 1999. Characterization of Mayven, a novel actin-binding protein predominantly expressed in brain. *Mol. Biol. Cell.* 10: 2361–2375.

Spradling, A.C. 1993. Developmental genetics of oogenesis. *In* The Development of *Drosophila melanogaster*. M. Bate and A. Martinez Arias, editors. Cold Spring Harbor Laboratory Press, Plainview, NY. 1–70.

Sun, S., M. Footer, and P. Matsudaira. 1997. Modification of Cys-837 identifies an actin-binding site in the beta-propeller protein scruin. *Mol. Biol. Cell.* 8:421–430.

Svitkina, T.M., and G.G. Borisy. 1999. Arp2/3 complex and actin depolymerizing factor/cofilin in dendritic organization and treadmilling of actin filament array in lamellipodia. *J. Cell Biol.* 145:1009–1026.

Tateno, M., Y. Nishida, and T. Adachi-Yamada. 2000. Regulation of JNK by Src during *Drosophila* development. *Science.* 287:324–327.

Theriot, J.A., and T.J. Mitchison. 1991. Actin microfilament dynamics in locomoting cells. *Nature.* 352:126–131.

Theurkauf, W.E., and T.I. Hazelrigg. 1998. In vivo analyses of cytoplasmic transport and cytoskeletal organization during *Drosophila* oogenesis: characterization of a multi-step anterior localization pathway. *Development.* 125:3655–3666.

Tilney, L.G. 1975. Actin filaments in the acrosomal reaction of *Limulus* sperm. Motion generated by alterations in the packing of the filaments. *J. Cell Biol.* 64:289–310.

Tilney, L.G., M.S. Tilney, and G.M. Guild. 1996. Formation of actin filament bundles in the ring canals of developing *Drosophila* follicles. *J. Cell Biol.* 133: 61–74.

Van Doren, M., A.L. Williamson, and R. Lehmann. 1998. Regulation of zygotic gene expression in *Drosophila* primordial germ cells. *Curr. Biol.* 8:243–246.

Verkhusha, V.V., S. Tsukita, and H. Oda. 1999. Actin dynamics in lamellipodia of migrating border cells in the *Drosophila* ovary revealed by a GFP-actin fusion protein. *FEBS Lett.* 445:395–401.

Waites, C.L., A. Mehta, P.K. Tan, G. Thomas, R.H. Edwards, and D.E. Krantz. 2001. An acidic motif retains vesicular monoamine transporter 2 on large dense core vesicles. *J. Cell Biol.* 152:1159–1168.

Way, M., M. Sanders, C. Garcia, J. Sakai, and P. Matsudaira. 1995. Sequence and domain organization of scruin, an actin–cross-linking protein in the acrosomal process of *Limulus* sperm. *J. Cell Biol.* 128:51–60.

Xue, F., and L. Cooley. 1993. *Kelch* encodes a component of intercellular bridges in *Drosophila* egg chambers. *Cell.* 72:681–693.

Yue, L., and A.C. Spradling. 1992. *Hu-li tai shao*, a gene required for ring canal formation during *Drosophila* oogenesis, encodes a homolog of adducin. *Genes Dev.* 6:2443–2454.

Zhai, L.W., P. Zhao, A. Panebra, A.L. Guerrerio, and S. Khurana. 2001. Tyrosine phosphorylation of villin regulates the organization of the actin cytoskeleton. *J. Biol. Chem.* 276:36163–36167.